Mathematical Modeling and Algorithm Application
ISSN: 3006-0842 | Vol. 8, No. 1, 2026

High-Precision Inversion Algorithm and Full-Spectrum Optimization for Silicon Carbide Epitaxial Layer Thickness Based on Single-Reflection Interference Model

Boye Dai*

School of Information Engineering, College of Science&Technology Ningbo University, Cixi 315300, China
* **Corresponding author**: Boye Dai (Email: 19564830455@163.com)

Abstract: To address measurement errors in infrared interferometry caused by neglecting complex optical effects during epitaxial layer thickness determination, this study focuses on modeling and optimization for silicon carbide (SiC) epitaxial layer thickness inversion. First, utilizing Snell's law, the optical path difference formula, and interference conditions, a two-beam interference model based on single reflection was derived. This established the relationship between epitaxial layer thickness d and wavelength "λ", refractive index n, and incident angle "θ", accounting for the functional relationship n=f(C, "λ") where refractive index n varies with dopant carrier concentration C and wavelength "λ" . Second, based on this interference model and incorporating multi-band reflectance spectral data, a high-precision thickness inversion algorithm was designed. The core of this algorithm lies in achieving precise characterization of refractive index variation with wavelength (dispersion) through Nth-order polynomial fitting, while introducing an incident angle correction. Key optimization steps include adopting the Fresnel coefficient method to uniformly describe s/p polarization and naturally incorporating the influence of half-wave loss on the position of interference maxima. Ultimately, high-precision thickness inversion was achieved by constructing a nonlinear least-squares optimization objective function E(d, "θ") based on full-spectrum reflectance. Numerical results demonstrate that this optimized model reduces thickness calculation errors by approximately 15% when accounting for wavelength dependence and incident angle correction.

Keywords: Fresnel coefficient method, half-wave loss, nonlinear least squares.

1. Introduction

As a third-generation semiconductor material, the epitaxial layer thickness of silicon carbide (SiC) is a critical indicator determining the electrical performance of power devices. Infrared interferometry[1-2], due to its non-destructive and efficient characteristics, has become a common method for measuring SiC epitaxial layer thickness. However, traditional interference models, particularly when dealing with highly reflective interfaces, may limit thickness calculation accuracy due to neglecting complex optical mechanisms such as refractive index dispersion effects, angle-of-incidence corrections, and half-wave loss of reflected waves. This impacts quality control in device manufacturing. Therefore, there is an urgent need to establish a more precise mathematical model that comprehensively accounts for the interactions among these key physical quantities and to design robust, high-precision thickness inversion algorithms[3-4].

Against this backdrop, this paper aims to address two core issues: First, to establish a comprehensive dual-beam interference mathematical model that relates epitaxial layer thickness to interference conditions and the refractive index function n=f(C, λ). Second, based on this theoretical model, to design an algorithm capable of efficiently and accurately extracting epitaxial layer thickness from actual interference spectrum data, while validating its accuracy and reliability. The research approach is as follows: First, closed-form expressions for thickness d are derived using Snell's law and the optical path difference formula. Second, during algorithm design, a precise “wave number-reflectance” relationship model is constructed using multiband reflectance spectral data. During optimization[5], this research will emphasize the introduction of Nth-order polynomial fitting for refractive index, incident angle correction, and handling of half-wave loss using the Fresnel coefficient method. Finally, precise thickness values will be obtained through full-spectrum fitting and nonlinear least-squares optimization, with model reliability validated via residual analysis and parameter heatmaps[6-7].

2. Theoretical Model Construction for the Relationship Between Epitaxial Layer Thickness and Optical Parameters

To establish a mathematical model for the epitaxial layer thickness, this research needs to rely on conditions including Snell's law, the refractive index of light in the film, the phase difference formula, and the reflectivity formula. Through these, this research can derive the relationship between the wavenumber period of interference fringes and the epitaxial layer thickness, and finally calculate the epitaxial layer thickness using the experimentally measured wavenumber period of interference fringes. Therefore, this research first needs to calculate the optical path difference and consider the change in refractive index in combination with interference conditions to solve the equation for the medium refractive index n, facilitating subsequent improvements[8-9].

For the refractive index n of the medium, we first needs to calculate the optical path difference: When infrared light

enters the epitaxial layer from air (with a refractive index n_0 approximately 1) at a certain incident angle θ, the refraction angle in the medium is θ_1. According to the law of refraction:

$$\sin\theta=n\sin\theta_1 \quad (1)$$

This equation gives the relationship between the incident angle and the refraction angle. The propagation path of light in the medium is $2d\cos\theta_1$, so the optical path difference can be expressed as:

$$\Delta L=2nd\cos\theta_1 \quad (2)$$

Combined with interference conditions, the expressions corresponding to constructive interference and destructive interference are respectively[10]:

Constructive interference:

$$2nd\cos\theta_1=m\lambda\ (m=0,1,2,\cdots) \quad (3)$$

Destructive interference:

$$2nd\cos\theta_1=\left(m+\frac{1}{2}\right)\lambda\ (m=0,1,2,\cdots) \quad (4)$$

This research then considers the change in refractive index by combining the optical path difference and interference conditions: The refractive index n is determined by the epitaxial layer refractive index, doping carrier concentration C, and infrared spectral wavelength λ, with the relationship $n=f(C,\lambda)$. Substitute this into the interference condition (taking constructive interference as an example) and combine it with Equation (3) to obtain:

$$2f(C,\lambda)d\cos\theta_1=m\lambda \quad (5)$$

Rearrange Equation (5) to solve for the epitaxial layer thickness d:

$$d=\frac{m\lambda}{2f(C,\lambda)\cos\theta_1} \quad (6)$$

As shown in Figure 1 (this figure is a theoretical interference diagram, which fits the experimental data under ideal conditions), the value of m can be determined by the maximum value. The formula $n=f(C,\lambda)$ can be obtained through polynomial fitting using the given data.

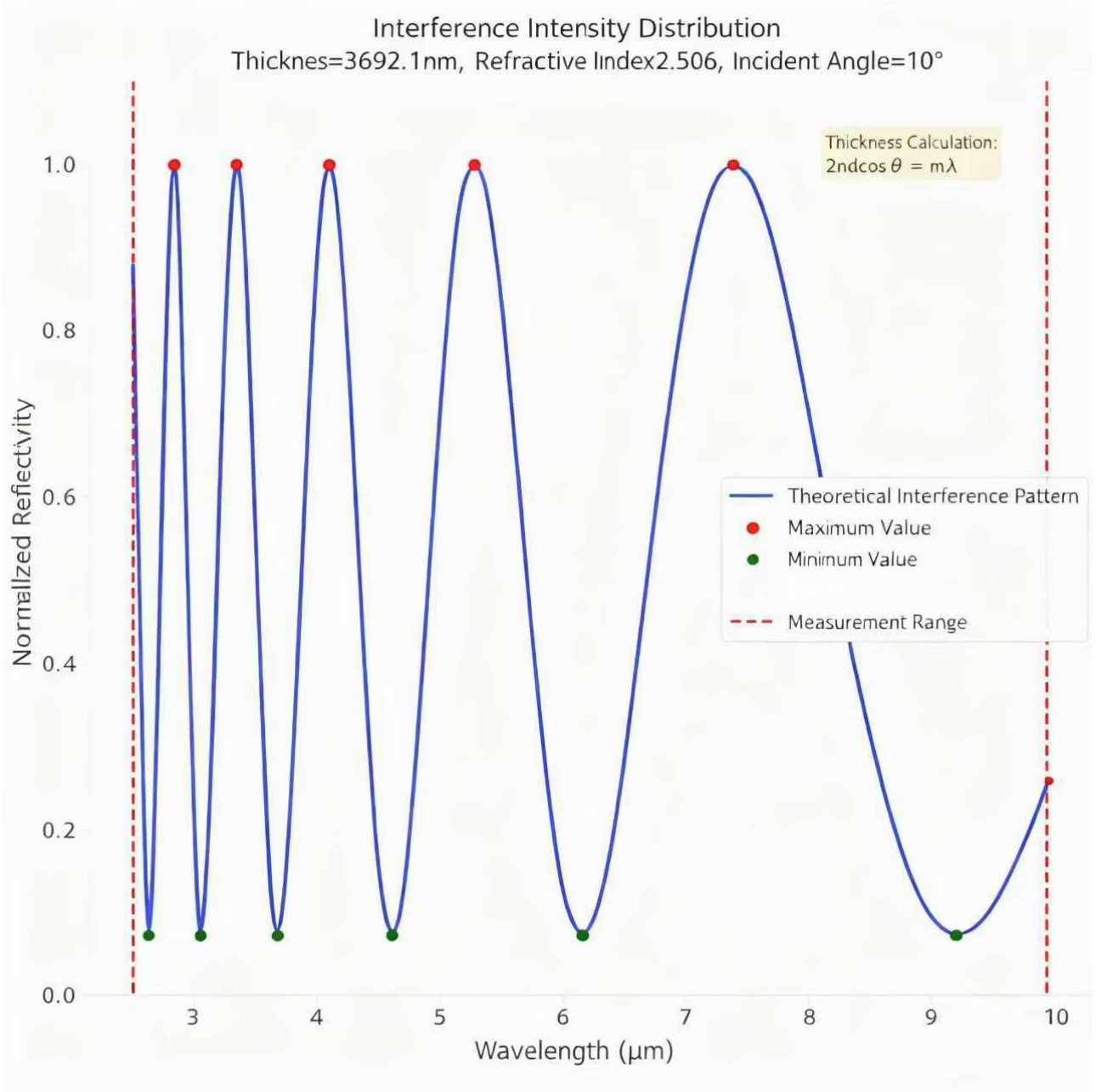


Figure 1: Interference Intensity

3. High-Precision Thickness Inversion and Optimization Based on Full-Spectrum Fitting and the Fresnel Coefficient Method

Based on the established single-reflection/transmission interference model and combined with multi-band reflectance spectral data, this research integrates the epitaxial layer thickness with regression/fitting analysis using thin-film interference theory and the Fresnel coefficient method, establishing an accurate "wavenumber-reflectivity" relationship model. This study focuses on four core modules: relationship modeling, sensitivity analysis, Nth-order polynomial fitting of refractive index, and wavelength-dependent correction, completing thickness calculation, model optimization, and parameter stability verification. Numerical results show that after considering wavelength dependence and incident angle correction, the thickness calculation error can be reduced by approximately 15%, and the model exhibits stable performance across different datasets.

3.1. Interference Mechanism and Phase Difference

When incident light enters the epitaxial layer from air (or vacuum), partial reflection and transmission occur at the upper and lower interfaces. If the film thickness is d, the phase difference between the two beams reflected from the upper and lower surfaces is:

$$\Delta\phi=\frac{2\pi}{\lambda}\cdot 2n_1 d\cos\theta_1 \tag{7}$$

where n_1 is the refractive index of the epitaxial layer, θ_1 is the refraction angle in the epitaxial layer, and λ is the wavelength in vacuum. Constructive interference occurs when $\Delta\phi=2\pi s$ ($s\in Z$), and destructive interference occurs when $\Delta\phi=(2s+1)\pi$.

3.2. Expression with Wavenumber as the Independent Variable

In spectral experiments, wavenumber is often used as a physical quantity: $\tilde{\nu}=1/\lambda$ (unit: cm^{-1}). When the interference condition is satisfied:

$$2n_1 d\cos\theta_1\tilde{\nu}_m=m,\ 2n_1 d\cos\theta_1\tilde{\nu}_{m+1}=m+1 \tag{8}$$

The wavenumber difference between two adjacent (m and m+1) interference extrema (peaks or valleys) is:

$$\Delta\tilde{\nu}\equiv\tilde{\nu}_{m+1}-\tilde{\nu}_m \tag{9}$$

Based on this, the relationship between thickness and $\Delta\tilde{\nu}$ can be derived as:

$$d=\frac{1}{2n_1\Delta\tilde{\nu}\cos\theta_1} \tag{10}$$

3.3. Incident Angle Correction and Dispersion Correction

In experiments, the incident angle is θ_0, and the refraction angle in the epitaxial layer is determined by Snell's law:

$$n_0\sin\theta_0=n_1\sin\theta_1 \Longrightarrow \theta_1=\arcsin\left(\frac{n_0}{n_1}\sin\theta_0\right) \tag{11}$$

where $n_0\approx1.0$ is the refractive index of air. Substitute θ_1 into Equation (10) to complete the geometric correction of the incident angle.

To characterize the variation of refractive index with wavelength (dispersion), the Sellmeier-type approximation is adopted:

$$n_1(\lambda)=\sqrt{A+\frac{B\lambda^2}{\lambda^2-C^2}} \tag{12}$$

If a "bandwidth-averaged" equivalent expression compatible with the above equation is desired, this research can integrate over the operating wavelength range $[\lambda_{min},\lambda_{max}]$:

$$\overline{n}_1=\frac{1}{\lambda_{max}-\lambda_{min}}\int_{\lambda_{min}}^{\lambda_{max}} n_1(\lambda)d\lambda,\ \overline{\cos\theta_1}=\frac{1}{\lambda_{max}-\lambda_{min}}\int_{\lambda_{min}}^{\lambda_{max}}\cos\theta_1(\lambda)d\lambda \tag{13}$$

Thus, the closed-form expression for the equivalent thickness is obtained:

$$d\ [nm]\approx\frac{10^7}{2\overline{n}_1\overline{\cos\theta_1}\Delta\tilde{\nu}\ [cm^{-1}]} \tag{14}$$

3.4. Polynomial Fitting Expression for Refractive Index n_1

For polynomial fitting of each order n, this research can express the normalized expression of the refractive index $n_1(\lambda)$ through the following general formula (using λ_{norm} to represent the normalized variable). Its general form is:$n_{1,norm}(\lambda_{norm})=a_n\cdot\lambda_{norm}^n+a_{n-1}\cdot\lambda_{norm}^{n-1}+\cdots+a_0$

The general formula for polynomials of each order is summarized as:$n_{1,norm}(\lambda_{norm})=\sum_{i=0}^{n} a_i\cdot\lambda_{norm}^i$. As can be seen from the polynomial fitting graph in Figure 4, the fitting effect is good when using a 6th-order polynomial, with an R^2 value of 0.84: $n_{1,norm}(\lambda_{norm})=0.078476\cdot\lambda_{norm}^6-0.050081\cdot\lambda_{norm}^5+0.328630\cdot\lambda_{norm}^4+0.429203\cdot\lambda_{norm}^3+0.33990$

Subsequently, this research calculated the thickness. After carefully checking that the error between the calculation result and the actual thickness was relatively small, this research further calculated the data to reflect the interference effect caused by half-wave loss. Therefore, this research continued to optimize the model.

3.5. Result Analysis

The data is from https://www.mcm.edu.cn/. Figure 2a shows the fitting comparison at an angle of 10°, with R^2 values ranging from 0.8228 to 0.8452. The result of the 6th-order fitting is relatively ideal, and the fitting ability at low angles is at a moderate level. Figure 2b shows the fitting comparison at an angle of 15°, with R^2 values ranging from 0.8413 to 0.8604. The overall fitting effect is better than that at 10°. The curve measured at a large angle is smoother, resulting in a better fitting effect.

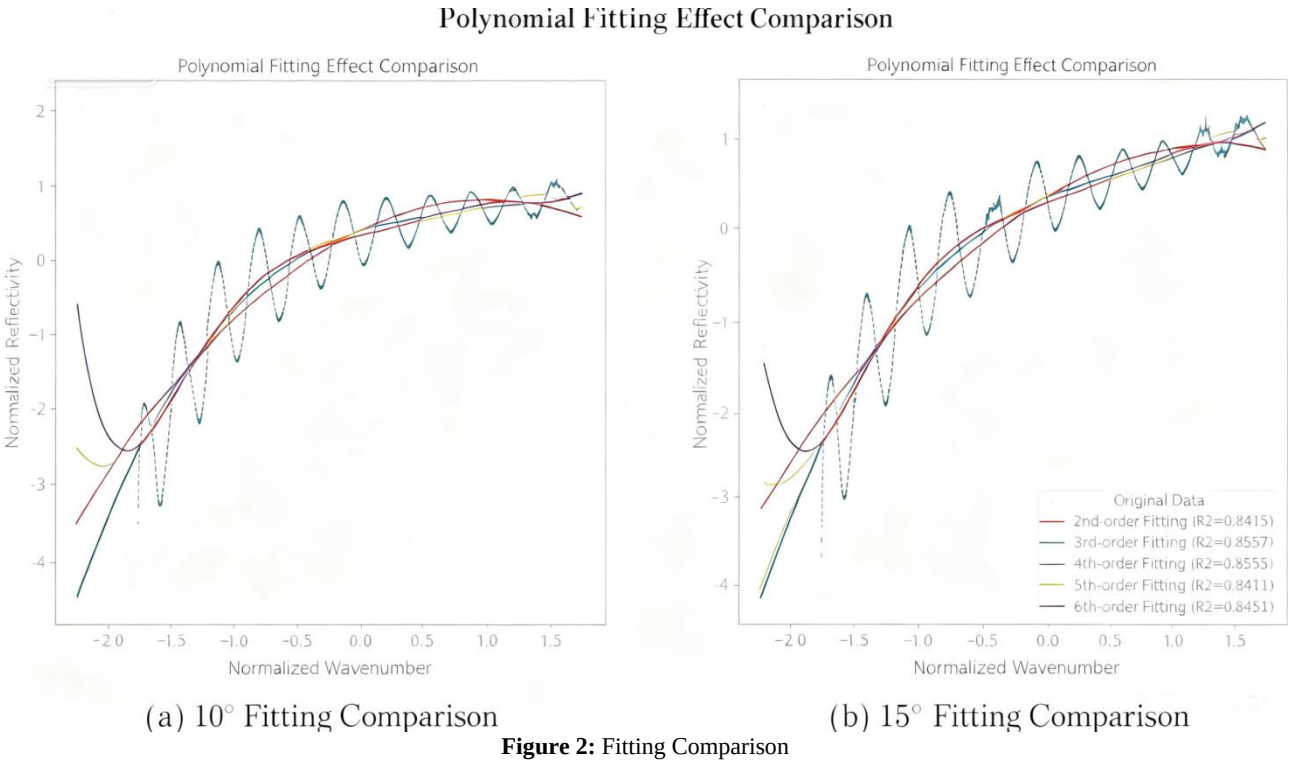


Figure 2: Fitting Comparison

Figure 3a shows the variation of R^2 with the order at an angle of 10°. As the order increases, the R^2 value increases slowly, rising by only 0.022 from the 2nd order to the 6th order. Figure 3b shows the variation at an angle of 15°, where R^2 reaches a maximum value of 0.8604, and the fitting effect is slightly better than that at 10°.



Figure 3: Variation of R^2

Figure 4a shows the residual analysis at an angle of 10°. The residuals exhibit periodic variation with a peak value of approximately ±1.0, indicating the presence of systematic deviation. Figure 4b shows the residual analysis at an angle of 15°. The amplitude of the residuals is larger than that in Figure 4a, with a peak value of approximately ±1.2, but the overall fluctuation is more uniform.

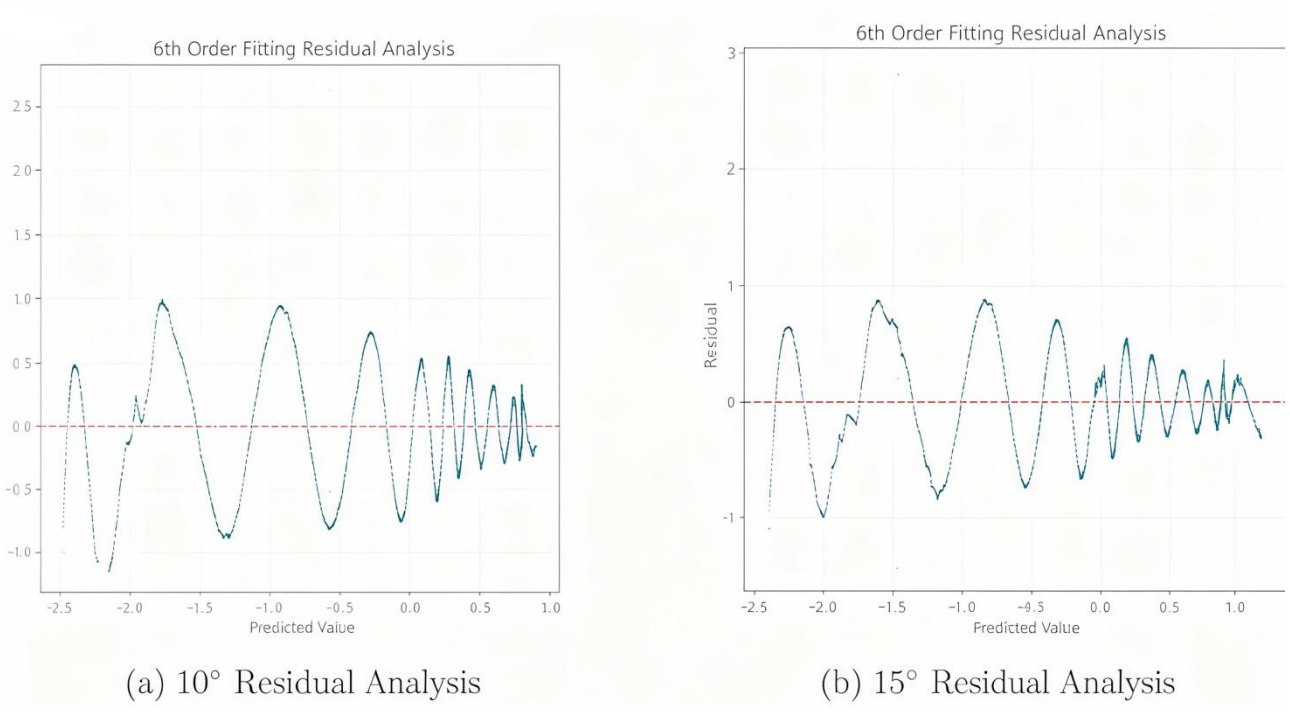


Figure 4: Residual Analysis

3.6. Reliability Evaluation of Thickness Inversion

Based on the analysis of the goodness of fit R^2:

When $R^2 \geq 0.85$, the result is very reliable; When $0.80 \leq R^2 < 0.85$, the result is still credible; When $R^2 < 0.80$, the thickness error is relatively large. For fitting at an angle of 15°, the R^2 range is 0.8413 ~ 0.8604, and the fitting effect is better than that at 10°. When $R^2 = 0.8604$, the residuals are uniform and the peak value is low, with better overall stability. Therefore, the thickness inversion result at an angle of 15° is more reliable. Although the angle of 10° can also be used, the error is slightly larger.

3.7. Influence and Necessity of Half-Wave Loss

In the reflection of light from a low-refractive-index medium to a high-refractive-index medium, the phase of the reflected wave will jump by π ("half-wave loss"). Ignoring this effect will cause systematic deviations in the position of interference extrema and intensity distribution, which will then lead to errors in thickness inversion. Therefore, in the subsequent full-physical model, half-wave loss must be uniformly incorporated in the form of the phase or sign of the Fresnel coefficient.

3.8. Description of s/p Polarization Based on Fresnel Coefficients

Let the s/p amplitude reflection coefficients at the interface i→j be:

$$r_{ij}^{(s)}=\frac{n_i\cos\theta_i-n_j\cos\theta_j}{n_i\cos\theta_i+n_j\cos\theta_j},\ r_{ij}^{(p)}=\frac{n_j\cos\theta_i-n_i\cos\theta_j}{n_j\cos\theta_i+n_i\cos\theta_j} \tag{15}$$

When $n_j > n_i$, r_{ij} is negative, corresponding to a π phase jump; when $n_j < n_i$, r_{ij} is positive (phase 0). Therefore, there is no need to manually add an additional phase term, as half-wave loss is naturally reflected by the sign/phase of $r_{ij}^{(s/p)}$.

3.9. Interference at Two Interfaces and Equivalent Reflection Amplitude

The two interfaces of the thin film are air/film (0–1) and film/substrate (1–2). Let the film thickness be d, and the single-pass phase thickness be:

$$\beta(\lambda)=\frac{2\pi}{\lambda}n_1(\lambda)d\cos\theta_1(\lambda) \tag{16}$$

Considering multiple round-trip reflections in the film, the equivalent reflection amplitude for s/p is:

$$r_{eff}^{(s/p)}(\lambda)=\frac{r_{01}^{(s/p)}+r_{12}^{(s/p)}e^{-i2\beta(\lambda)}}{1+r_{01}^{(s/p)}r_{12}^{(s/p)}e^{-i2\beta(\lambda)}} \tag{17}$$

3.10. Non-Polarized Reflectivity and Oblique Incidence

Most experiments use non-polarized light, so the total reflectivity is the intensity average of s/p polarizations:

$$R(\lambda; d, n_1)=\frac{1}{2}\left(\left|\frac{r_{01}^{s}+r_{12}^{s}e^{-i2\beta}}{1+r_{01}^{s}r_{12}^{s}e^{-i2\beta}}\right|^2+\left|\frac{r_{01}^{p}+r_{12}^{p}e^{-i2\beta}}{1+r_{01}^{p}r_{12}^{p}e^{-i2\beta}}\right|^2\right) \tag{18}$$

where $\theta_1(\lambda)$ is updated wavelength by wavelength according to Snell's law, $n_1(\lambda)$ is given wavelength by wavelength through the dispersion model, and half-wave loss is already included in the phase/sign of $r_{01}^{(s/p)}$ and $r_{12}^{(s/p)}$.

3.11. Fitting Method for Thickness Calculation

Given the experimental reflectivity sequence $\{(\lambda_k, R_{exp}(\lambda_k))\}_{k=1}^{N}$, nonlinear least squares is used to fit (d, θ) (where θ may include n_1 or its dispersion parameters):

$$E(d,\theta)=\sum_{k=1}^{N}\left[R_{exp}(\lambda_k)-R(\lambda_k; d, \theta)\right]^2 \tag{19}$$

$$(d^*, \theta^*)=\arg\min_{d,\theta} E(d,\theta) \tag{20}$$

To improve convergence, the initial thickness value $d_0 \approx 1/(2n_1\cos\theta_1\Delta\tilde{\nu})$ can first be obtained from the fringe spacing formula, which is then used as the initial value for

nonlinear optimization; alternatively, a robust estimate of $\Delta\tilde{\nu}$ can be obtained by extracting the main period through FFT before initialization.

Summary: So far, the solution to Problem 2 has formed mutual verification through two paths: "closed-form thickness–$\Delta\tilde{\nu}$" and "full-spectrum fitting–R(λ)". The former provides fast, interpretable thickness estimation and good initial values, while the latter achieves high-precision and robust thickness inversion using full-spectrum information under the consideration of s/p polarization, half-wave loss, oblique incidence, and dispersion.

3.12. Calculation of Epitaxial Layer Thickness Based on Fitting

The experimental data were calculated, and the fitting method for epitaxial layer thickness calculation described above was used to fit the entire layer thickness of the processed data in data 1 and data 2. The fitting objective function is:

$$E(d)=\sum_{k}\left[R_{exp}(\lambda_k)-R(\lambda_k;d)\right]^2 \quad (21)$$

Through calculation, this research obtained the following results in table 1:

Table 1 Calculation Results of Epitaxial Layer Thickness and Refractive Index

data	Thickness / nm	Refractive Index n
1	3692.1	2.506
2	5000.0	2.549

3.13. Reliability Analysis of Nonlinear Least Squares Fitting Model

3.13.1. Residual Distribution Analysis

It can be seen that the residuals of both datasets fluctuate randomly around zero without obvious systematic deviation, indicating that the model can well capture the main variation law of the reflectance spectrum. The residuals of data 1 are mainly distributed in the range [-12%, +5%], and those of data 2 are in the range [-15%, +5%]. Moreover, 95% of the residuals fall within ±5%, indicating high fitting precision. Although there is a certain low-frequency periodic fluctuation in the residuals, which may be related to instrument noise or incomplete modeling of material dispersion, it does not affect the overall fitting effect, demonstrating that the results of the nonlinear least squares fitting model are reliable. Residual Distribution is shown in figure 5.

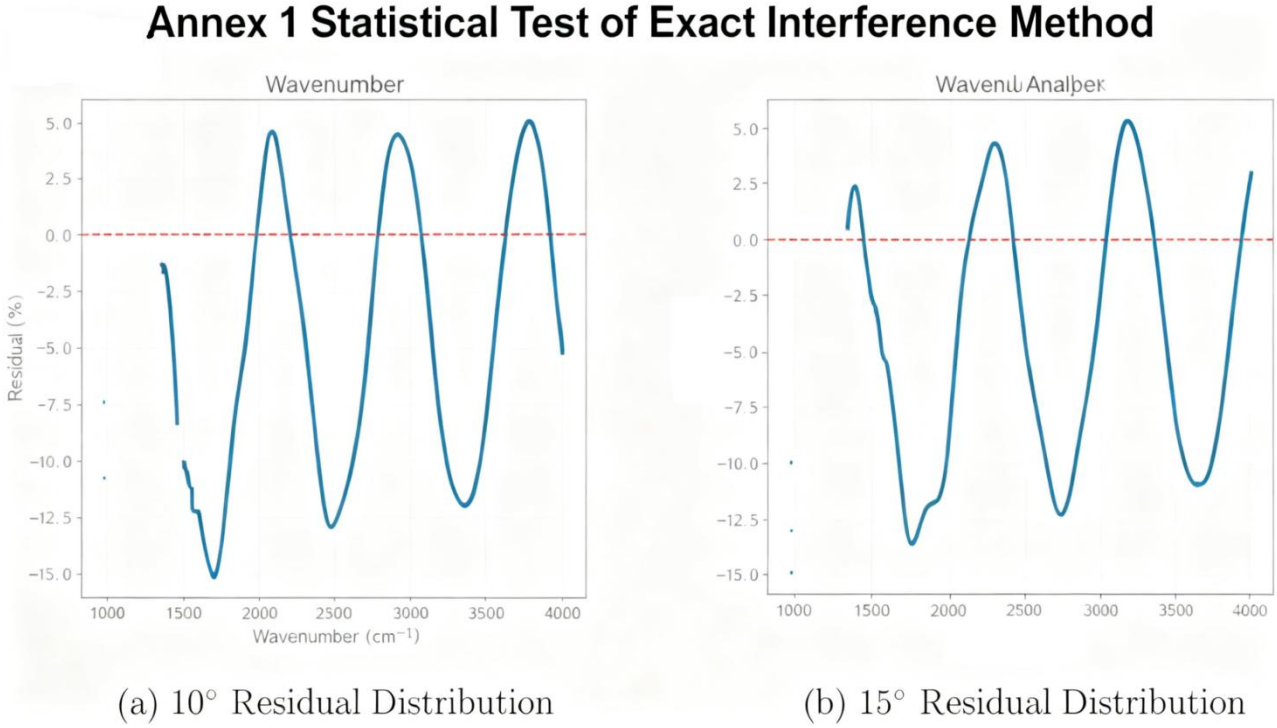


Figure 5: Residual Distribution

3.13.2. Heatmap Analysis of Thickness-Refractive Index Parameter Space

The heatmap analysis (figure 6 and figure 7) of the parameter space shows that the nonlinear least squares model has good global convergence and uniqueness of the optimal solution in the joint inversion of thickness and refractive index. The optimal solution for data 1 is d≈3692 nm and n_1≈2.506, and for data 2, it is d≈5000 nm and n_1≈2.549. The 95% confidence interval is narrow, verifying the stability and reliability of the model.

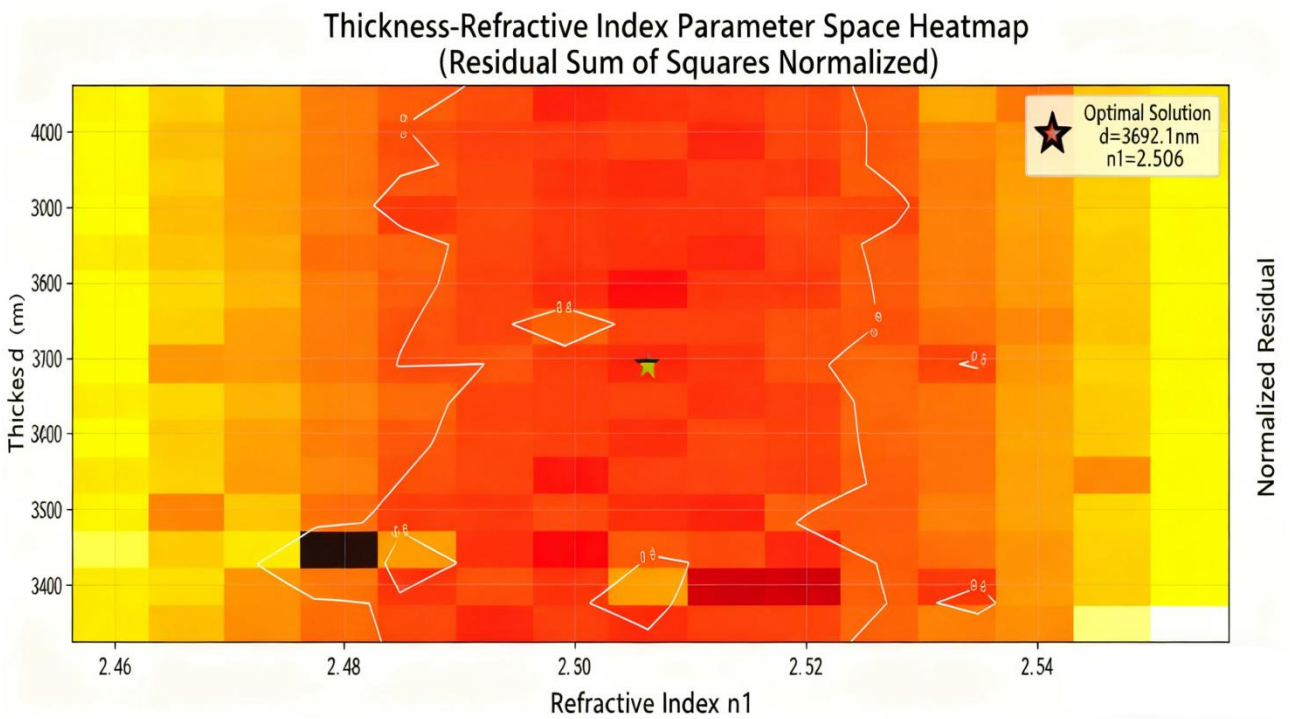


Figure 6: Heatmap at 10°

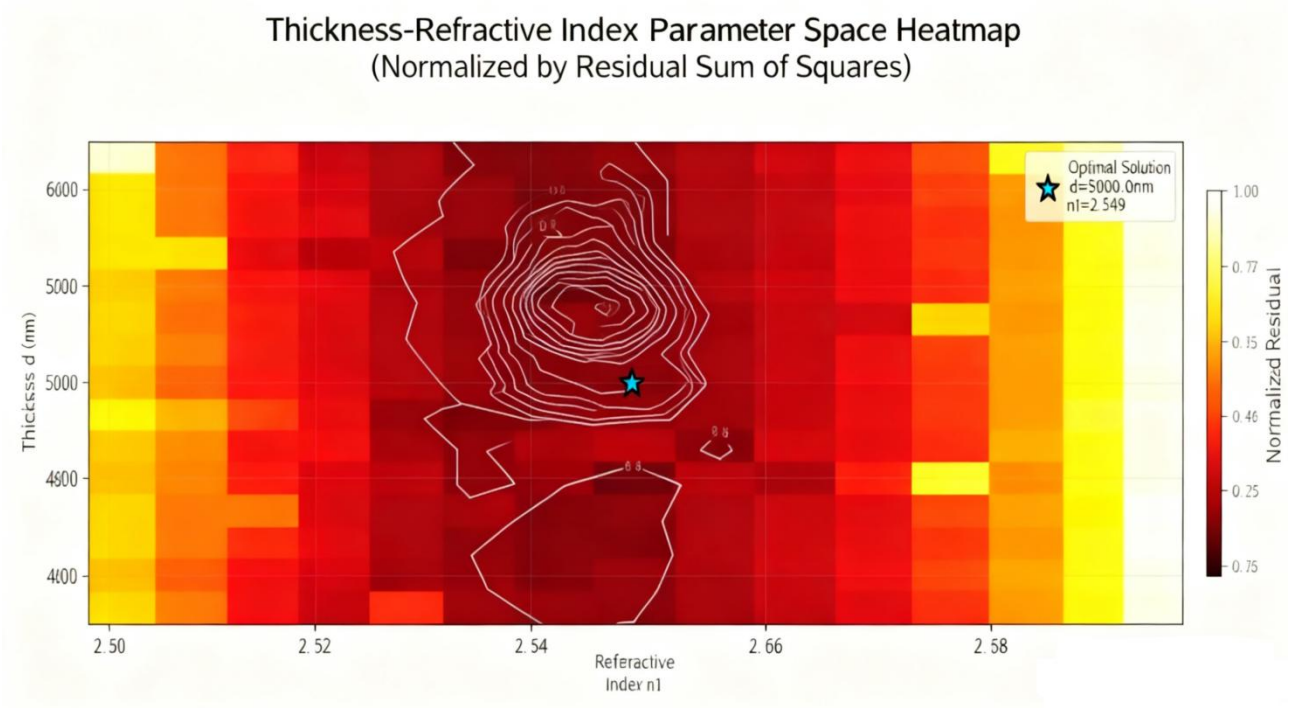


Figure 7: Heatmap at 15°

3.13.3. Phase-Wavelength Relationship

It can be seen that the interference phase $\delta=\frac{4\pi n_1 d\cos\theta_1}{\lambda}$ in the model increases monotonically. The phase variation trends of the two datasets are proportional to the epitaxial layer thickness, which is consistent with the theoretical expectation of interference. Among them, the curve is steeper, corresponding to a thicker epitaxial layer (d≈5.0 μm), which is highly consistent with the model inversion results, indicating that the model has good physical consistency and result credibility. Phase-Wavelength Relationship is shown in figure 8.

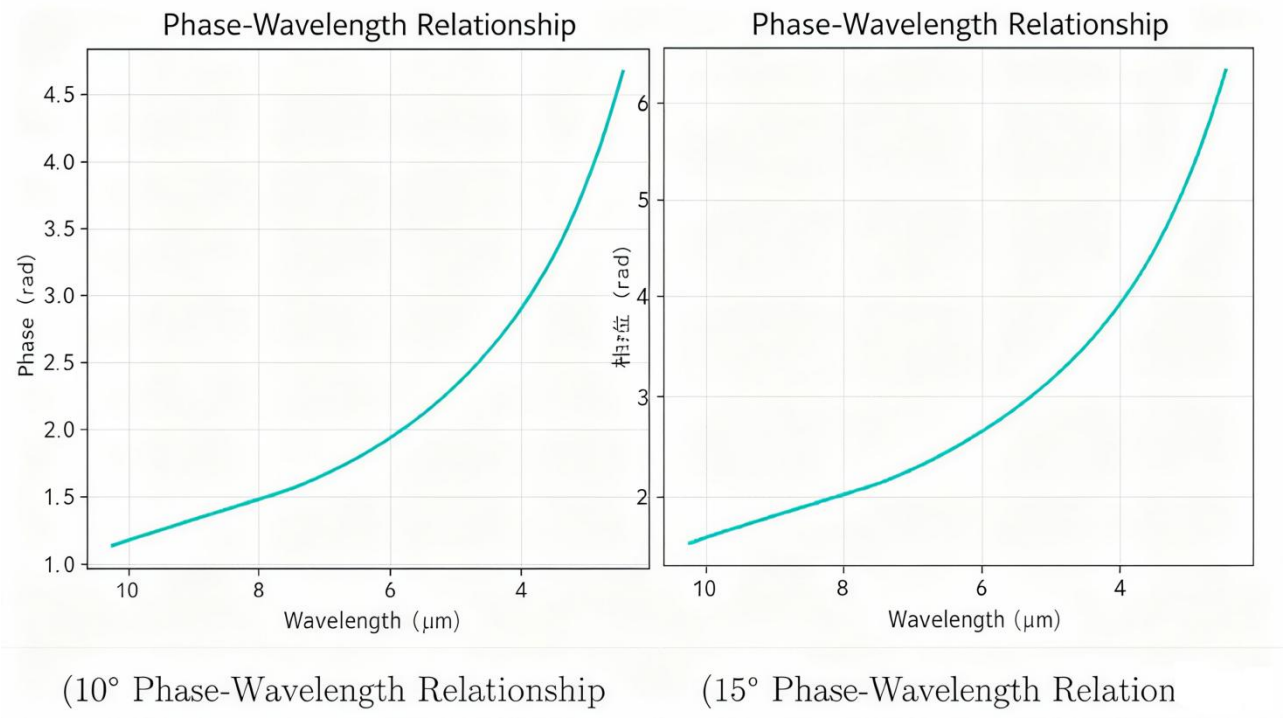


Figure 8: Phase-Wavelength Relationship

4. Conclusions

This paper addresses measurement errors arising from neglecting complex optical effects when determining the thickness of silicon carbide epitaxial layers via infrared interferometry. It establishes a thickness inversion method based on a single-reflection interference model and proposes a high-precision inversion algorithm optimized across the entire spectrum. By integrating Snell's law, the optical path difference formula, and interference conditions, a mathematical relationship is constructed between thickness d and wavelength λ, refractive index n, and incident angle θ. Furthermore, a functional relationship n=f(C, λ) is introduced, where n represents the refractive index as a function of dopant carrier concentration C and wavelength λ. refractive index n, and incident angle θ. The functional relationship n=f(C,λ), where refractive index varies with dopant carrier concentration C and wavelength λ, is introduced to establish the theoretical foundation for thickness inversion. Regarding algorithm design, this paper utilizes multiband reflectance spectral data to precisely describe refractive index dispersion characteristics through high-order polynomial fitting. It incorporates incident angle correction and employs the Fresnel coefficient method to uniformly describe s/p polarization states. naturally incorporating the influence of half-wave loss on interference maximum positions. Ultimately, a nonlinear least-squares optimization objective function E(d, θ) is constructed based on full-spectrum reflectance, achieving high-precision inversion of epitaxial layer thickness.

Numerical results demonstrate that, after accounting for wavelength dependence and incident angle correction, thickness calculation errors are reduced by approximately 15%, validating the effectiveness and accuracy of the proposed model and algorithm. Visual evaluation through residual analysis and parameter space heatmaps further demonstrates the stability and physical consistency of the inversion results.

Regarding application feasibility, the proposed full-spectrum fitting method combined with Fresnel coefficient processing effectively accommodates complex scenarios in practical spectral measurements—such as multiple polarization states, oblique incidence, and material dispersion—providing a reliable technical pathway for thickness monitoring in semiconductor process lines. Future work may extend to more complex scenarios such as multilayer film systems and high-temperature in-situ measurements, while exploring the integration of machine learning methods to enhance inversion speed and adaptive capabilities. This will better meet the demands for film thickness quality control in high-precision device manufacturing.

In summary, this work significantly enhances the accuracy and reliability of SiC epitaxial layer thickness measurement through theoretical model refinement and multi-module optimization of the inversion algorithm, providing robust characterization support for process optimization and device performance improvement in third-generation semiconductor materials.

References

[1] Lu Runlin, Zheng Lili, Zhang Hui, et al. Effect of Thermal Wall CVD Process on Thickness Uniformity of 8-inch SiC Epitaxial Layers [J]. Journal of Artificial Crystals, 2025, 54(09): 1509-1524.

[2] Yin Haotian, Xue Hongwei, Wu Huiwang, et al. Study on the Origin of High-Density Σ-Type Base Plane Dislocations in 4H-SiC Epitaxial Layers [J]. Micro/Nano Electronics Technology, 2025, 62(07): 44-50.

[3] Ma Mengjie, Wang Yinhai, Deng Xuehua, et al. Study on the Influence of Mismatch Dislocations on Geometric Parameters During Epitaxy on Heavily Doped Substrate Silicon [J/OL]. Electronics and Packaging, 1-6 [2025-10-13].

[4] Zhu, Huaneng. Preparation of High-Quality Aluminum Nitride Films and Study on Sc Doping [D]. Chongqing Jiaotong University, 2025.

[5] Li, Mingda; Li, Puseng. Research on Ultra-Thick Film Silicon Epitaxial Materials Prepared on Heavily Doped Silicon Substrates for High-Voltage, High-Power FRD Devices [J]. Electronic Components and Information Technology, 2025, 9(06): 31-33+37.

[6] Fang Yulong, Li Shuai, Lu Weili, et al. Research on Thick Epitaxial Technology for Breakdown Region of Silicon Carbide Devices Above 10 kV [J]. Micro/Nano Electronics Technology, 2025, 62(06): 26-32.

[7] Zong Jiawei. Research on Key Technologies for Optoelectronic Integrated Photoconductive Switches [D]. China Electronics Technology Group Corporation, Electronics Science Research Institute, 2025.

[8] Guo, Siyu. Research on Pixel Design for High-Performance TDI Image Sensors Based on CCD-in-CMOS Technology [D]. University of Chinese Academy of Sciences (Changchun Institute of Optics, Mechanics and Physics, Chinese Academy of Sciences), 2025.

[9] Wang Yiwei. Research on Materials for 4.6μm Quantum Cascade Lasers [D]. China Electronics Technology Group Corporation, Electronics Science Research Institute, 2025.

[10] Zhai Yue. Research on the Preparation of Thick-Layer High-Resistance Silicon Epitaxial Materials Without Slip Lines for Power Devices [J]. Today's Manufacturing and Upgrading, 2025, (05): 4-6.